replicated by the one-dimensional simulation code HIMICO[9,10]. Comparison between Figs 2 and 3 gives a comprehensive view of two different modes.

Figure 4 shows how the neutron yields depend on the thickness of the target pusher. A higher yield is achieved as a consequence of effective acceleration on decreasing the thickness. With an increasing target diameter, a higher yield is expected. However, the neutron yields for the 950 μm/500 ps data are lower by an order of magnitude than those for the 950 μm/750 ps (Fig. 4), suggesting that the 500-ps pulse is too short for the shock-wave multiplexing in 950-μm targets. The important requirement for shock multiplexing is a continuous increase of pusher acceleration, which is determined by the target configuration and the laser intensity. Simulations allow us to predict an optimized condition. The best matching occurred at the combination of 950 μm/750 ps. We detected 1.25×10^{12} neutrons, whose energy corresponds to $\sim 10^{-3}$ of the absorbed energy.

The space-resolved X-ray spectroscopy measurements and the X-ray pinhole images conclusively show that the core is round (30% sphericity) and that the pusher does not mix with the fuel. Plausible mechanisms for stabilization may be: a decrease of the target aspect ratio during the implosion; and that of the Atwood number on pusher-fuel contact surface. These are caused by increase of the pusher aeral density by implosion. Possibility of the impact fusion is excluded by the fuel-temperature measurement. The temperatures deduced from the neutron time-of-flight measurements were 3–7 keV and increased with increasing target-aspect ratio.

We thank K. Mima, T. Yabe and the members of the experimental and theoretical groups at the Institute of Laser Engineering, Osaka University, who contributed to the physical arguments and experimental data described here.

Received 22 November 1985; accepted 16 January 1986.

1. Yamanaka, C. *et al. 10th int. Conf. Plasma Phys. Controlled Nucl. Fusion Res.* (IAEA-BI-1, London, 1985).
2. Manes, K. R. *et al. Phys. Rev. Lett.* **39**, 281–284 (1977).
3. Godwin, R. P. *et al. Phys. Rev. Lett.* **39**, 1198–1201 (1977).
4. Kruer, W. L. in *Progress in Lasers and Laser Fusion* (eds Kursunoglu, B., Perlmutter, A. & Widmayer, S. M.) 5 (Plenum, New York, 1975).
5. Kidder, R. E. *Nucl. Fusion* **14**, 53–60 (1974).
6. Bertke, S. D. & Goldman, E. B. *Nucl. Fusion* **18**, 509–518 (1978).
7. Freeman, J. R., Clauser, M. J. & Thompson, S. L. *Nucl. Fusion* **17**, 223–230 (1977).
8. Hattori, F., Takabe, H. & Mima, K. *Phys. Fluids* (submitted).
9. Yabe, T. *et al. Nucl. Fusion* **21**, 803–816 (1981).
10. Kiyokawa, S. *et al. J. appl. Phys. Japan* **22**, L772–L774 (1983).

Observations of solitary waves in a viscously deformable pipe

David R. Scott*, David J. Stevenson† & John A. Whitehead Jr‡

* Seismological Laboratory and † Division of Geological and Planetary Sciences, California Institute of Technology, Pasadena, California 91125, USA
‡ Department of Physical Oceanography, Woods Hole Oceanographic Institution, Woods Hole, Massachusetts 02543, USA

We have made simple observations of the ascent of a buoyant fluid through a pipe formed in a denser and more viscous fluid that can deform viscously and allow the pipe radius to change. There is no wall between the two fluids, and the Reynolds number is small in both fluids. If the buoyant fluid is supplied at a uniform rate, the system exhibits uniform Poiseuille flow. The response of the system to fluctuations in the rate of supply of the buoyant fluid is to form local maxima in the pipe radius that ascend as solitary waves. Larger-amplitude waves can catch up and collide with smaller waves and, to a good approximation, both waves recover their original form and amplitude after such a collision. Periodic wavetrains are formed when the supply of fluid to the pipe is increased and sustained at a higher rate. These observations gain significance because the system is analogous to that of one-dimensional buoyancy-driven porous flow in a viscous matrix. The experiment may be regarded as a laboratory analogue for studying some aspects of the equations governing porous flow. The observed behaviour is consistent with recent theoretical and computational studies[1,2], which have focused on the problem of magma migration in the Earth. The behaviour we observe will, however, arise in other systems governed by the same mechanics. The existence of solitary waves in such systems means that the responses to transient changes in the porosity or the supply of fluid could be long-lived.

Our interest in this sytem arises from recent advances[3] in the understanding of the segregation of magma from a porous matrix of residual crystals, an important process in the crust and mantle of the Earth. Observations of the texture of partially molten rocks[4,5] have shown that the network of melt may remain interconnected down to very small volume fractions of melt. Recent work identifies the importance of compaction: the deformation of the porous matrix through which the buoyant melt rises. This work, summarized by McKenzie[6], has prompted the formulation of a system of equations governing the movement of a buoyant fluid through a porous, deformable matrix; the latter property is essential if magma is to escape from a closed region of partial melt. Our experiment reproduces the essential mechanics of the more complex porous flow problem, and is of interest to those studying porous systems other than partially molten rock.

The experimental apparatus is very simple and can be reproduced easily. A transparent tank, $\sim 10\ \text{cm} \times 10\ \text{cm} \times 50\ \text{cm}$ high, contains transparent viscous fluid. This fluid forms the walls of the deformable pipe. To form the pipe, a buoyant fluid that is less viscous is introduced through a nozzle in the centre of the base of the tank. This fluid is supplied from a reservoir with a variable-pressure head, or by a low-rate pump such as a syringe driver. The buoyant fluid is dyed to make the pipe clearly visible. The experimental fluids we have used are different mixtures of clear honey and water. Diluting honey with water produces a mixture that is less dense and less viscous than pure honey. In Figs 1, 2, the denser fluid in the tank is 100% honey (density $1.42\ \text{g cm}^{-3}$, viscosity 80 poise), and the buoyant fluid in the pipe is 77% honey (density $1.31\ \text{g cm}^{-3}$, viscosity 0.6 poise). The use of mutually-soluble fluids eliminates the effects of surface tension. We have determined that diffusion of water between the two fluids is negligible in the experiment. The use of different mixtures of corn syrup and water also provides good results.

The first part of the buoyant fluid to be introduced ascends as a diapir, but as more fluid is supplied a pipe is established between the nozzle and the top of the tank[7]. If the pressure head of the reservoir of buoyant fluid is held constant, a state of steady Poiseuille flow is established. In this state, the pressure head almost balances the resistance in the tubing supplying the nozzle, because the Reynolds number is small, so there is no pressure difference between the two fluids in the tank. Within the pipe, the buoyancy force balances the non-hydrostatic pressure gradient. We typically use pipe diameters of a millimetre or two.

To create solitary waves, the rate of supply of fluid to the stable pipe must be increased. This can be achieved by increasing the pressure head of the reservoir, or by increasing the supply rate from the syringe driver. In our experiments, the pipe has invariably responded to the change in supply rate by forming solitary waves or wavetrains.

If the increased supply is temporary, followed by a return to the original rate, solitary waves are formed. With care, it is possible to form a single solitary wave. The solitary wave ascends along the uniform pipe at a constant velocity, with unchanging

form. The pipe returns to its original uniform diameter after the passage of the wave. Although the waves are shape-preserving, they are dispersive in that they have an amplitude-dependent phase velocity. A consequence of this is that larger waves catch up and collide with smaller waves; remarkably, both waves survive such a collision almost unscathed (see Fig. 1).

If the increased supply is sustained, a periodic train of solitary waves is formed. This is best demonstrated using a syringe driver, because the rate of supply can be controlled precisely. Figure 2 shows the results of such an experiment. The response to a simple step between two uniform supply rates is a long-lived wavetrain. This differs from the varicose instability[8], which occurs when the Reynolds number in the interior fluid exceeds a value[9] of ~8. In this experiment, the maximum Reynolds number is about 3, and the formation of wavetrains is readily observed at smaller Reynolds numbers.

The theoretical model that we have used to compare with the experiments describes the behaviour of fluctuations in the diameter of a single, uniform vertical pipe in an infinite medium. We refer to the viscous wall fluid as the solid phase, and the fluid in the pipe as the liquid. The rigorous description of this system appears to be analytically intractable, but a good approximation can be obtained as follows. As the Reynolds number is small, both in the solid and the liquid, the velocity field satisfies the biharmonic equation and the pressure field satisfies Laplace's equation. If the walls of the tank are distant from the pipe, then the instantaneous pressure distribution in the solid can be represented as a sum of Fourier components of the form $K_0(kr)$ sin kz, where z is the vertical coordinate, r is the radial coordinate, k is the vertical wavenumber, and K_0 is the modified Bessel function of the second kind and zeroth order. We then find that a Fourier component of the radial flow in the solid around the pipe has, in the limit $kr \ll 1$, the form

$$v_r \propto \frac{1}{r} + O(kr^2 \ln kr) \tag{1}$$

We note that we seek *a priori* solitary wave solutions with some wavelength λ. In the limit where the solid viscosity η^s is much greater than the liquid viscosity η^l, we find that $2\pi a/\lambda \sim ka \ll 1$, where $a = a(z)$ is the pipe radius. The stress boundary condition at the pipe wall is then simple, since we need only take the $1/r$ term in the expansion of v_r above; the Fourier sum is trivial and the balance of normal stress across the pipe wall is approximated by

$$p^l = p(z=0) - \rho^s g z + 2\eta^s \frac{v_r(a)}{a} \tag{2}$$

where ρ^s is the solid density, g is the acceleration due to gravity and v_r is now the total radial flow at $r = a$. The Poiseuille flow formula for the flow in the pipe, neglecting the slope of the walls, is

$$u = -\frac{\pi a^4}{8\eta^l}\left[\frac{\partial p^l}{\partial z} + \rho^l g\right] \tag{3}$$

where u is the volume flux of liquid through the pipe relative to the solid and ρ^l is the liquid density. We link the flow in the solid and liquid using continuity. Clearly, $v_r(a) = \partial a/\partial t$, where t is time. Also,

$$\frac{\partial u}{\partial z} = -\frac{\partial}{\partial t}(\pi a^2) \tag{4}$$

Substituting the z-derivative of equation (2) into equation (3) and using these continuity conditions, we obtain

$$u = \frac{\pi a^4}{8\eta^l}\left[g(\rho^s - \rho^l) + \eta^s \frac{\partial}{\partial z}\left(\frac{1}{\pi a^2}\frac{\partial u}{\partial z}\right)\right] \tag{5}$$

As expected, equations (4) and (5) are analogous to those governing porous flow in a deformable matrix, when the flow is constrained to one dimension (vertical). This similarity persists even if the tank walls are closer to the conduit and 'plug flow' occurs in the solid[10]. The pipe equations are obtained by substituting the porosity $f \equiv \pi a^2$, choosing an f^2 dependence for the permeability, and choosing a $1/f$ dependence for the bulk viscosity of the solid matrix.

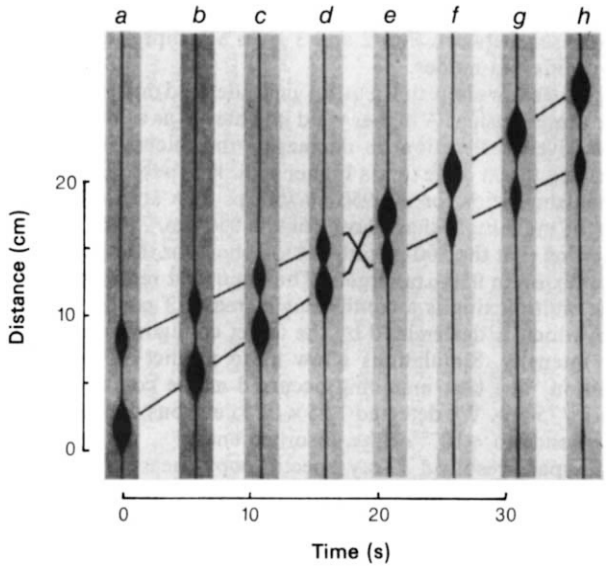

Fig. 1 The interaction of two solitary waves. The photographs were taken using back lighting and a flat-sided tank, to avoid distortion. Only part of the tank is shown in each frame; the tank is 10-cm wide. The frames are spaced according to their separation in time. In frames *a*–*c* and *f*–*h*, the two waves ascend as solitary waves with constant amplitude, shape and velocity. This is shown by the ruled lines. The main outcome of the interaction seen in frames *d*, *e* is the phase shift, shown by the offset of the ruled lines. The amplitudes of the two waves are conserved very well; our measurements show that the larger waves gain a little liquid at the expense of the smaller waves. The uniform pipe is undisturbed by either the passage of the waves or the interaction.

Some analysis, and numerical modelling, of solitary wave solutions to the one-dimensional porous flow equations has already been presented[1,11]. In particular, Scott and Stevenson[1] give explicit expressions for the dispersion relation between wave amplitude and phase velocity. For the special case of a deformable pipe, this relationship is:

$$c = \frac{a_0^2 g(\rho^s - \rho^l)}{8\eta^l} 2 \frac{\left[\ln \Psi - \frac{1}{2} + \frac{1}{2\Psi^2}\right]}{\left[1 - \frac{2}{\Psi} + \frac{1}{\Psi^2}\right]} \tag{6}$$

where a_0 is the radius of the uniform part of the pipe, c is the phase velocity and $\Psi = (a_{max}/a_0)^2$. The leading quotient on the right-hand side is the mean Poiseuille flow velocity in the uniform pipe.

Using photographs of the experiment, we have made limited measurements of the amplitudes, ascent velocities, and wavelengths of the waves; these agree with the theory to within 10%. Waves with values of Ψ between 6 and 80 were used. Thus, we find good agreement between measurements of this experiment, measurements of numerical experiments[1], and the theoretical dispersion relation. The experiments presented in Figs 1, 2 complement the numerical experiments presented earlier[1], where we similarly showed a collision and the formation of a wavetrain. This correspondence lends credibility to the numerical studies. We note that more detailed measurements have been carried out by Olson and Christensen[12].

Real porous media have a much more complicated micro-

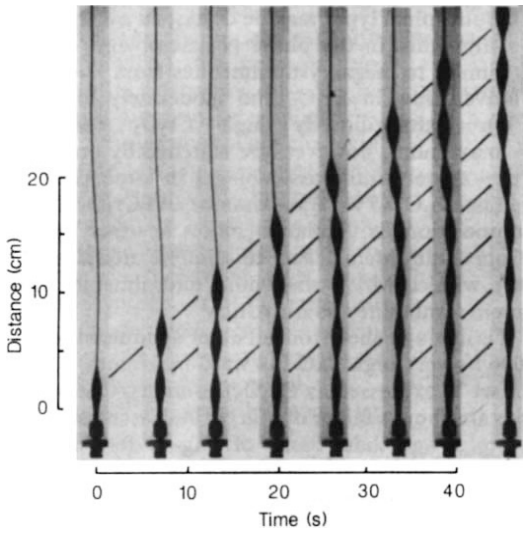

Fig. 2 The formation of a periodic wavetrain. This experiment started with a uniform pipe, sustained by a constant supply of buoyant liquid from the nozzle seen at the base of the frames. The rate of supply was then increased and held at a new constant level, approximately 220 times higher. This increase could be accommodated by the formation of a larger uniform pipe, but the system preferentially forms a periodic wavetrain. In longer experiments, the wavetrain does slowly degrade down to a larger uniform pipe. The ruled lines are parallel and equally spaced.

scopic structure than that discussed here; this will change the functional form of the matrix permeability and viscosity, but not the existence and nature of the waves described here. More importantly, real porous media are three-dimensional; numerical experiments[10] indicate that the one-dimensional waves are unstable in higher dimensions, but that solitary waves of higher dimensions are formed. The balance of dissipative mechanisms and gravitational energy release governing the ascent of these waves is the same in one, two, or three dimensions. We believe, therefore, that the experiments described here are not only pedagogically useful, but also serve as a laboratory analogue for real Earth processes. Specifically, we may expect the geochemistry, morphology, and timing of igneous processes to be affected by phenomena resembling those reported here: this is discussed elsewhere[10]. It is possible that solitary waves arise in other porous systems.

We thank Robert E. Frazel at Woods Hole, and various members of the Division of Geological and Planetary Sciences at Caltech, for experimental assistance. Peter Olson and Uli Christensen have independently performed experiments similar to those described here, and have shared their results. This work was supported by NSF grant EAR-8418353, and by the Geodynamics program of the Center for the Analysis of Marine Systems at Woods Hole Oceanographic Institution. Contribution number 4271, Division of Geological and Planetary Sciences, California Institute of Technology.

Received 29 September; accepted 30 December 1985.

1. Scott, D. R. & Stevenson, D. J. *Geophys. Res. Lett.* **11**, 1161-1164 (1984).
2. Richter, F. M. & McKenzie, D. P. *J. Geol.* **92**, 729-740 (1984).
3. McKenzie, D. P. *J. Petrol.* **25**, 713-765 (1984).
4. Waff, H. S. & Bulau, J. R. *J. geophys. Res.* **84**, 6109-6114 (1979).
5. Cooper, R. F. & Kohlstedt, D. L. *Tectonophysics* **107**, 207-233 (1984).
6. McKenzie, D. P. *Earth planet. Sci. Lett.* **74**, 81-91 (1985).
7. Whitehead, J. A. & Luther, D. S. *J. geophys. Res.* **80**, 705-717 (1985).
8. Whitehead, J. A. *Geophys. J. R. astr. Soc.* **70**, 415-433 (1982).
9. Huppert, H. E., Sparks, R. S. J., Whitehead, J. A. & Hallworth, M. A. *J. geophys. Res.* (in the press).
10. Scott, D. R. & Stevenson, D. J. *J. geophys. Res.* (in the press).
11. Barcilon, V. & Richter, F. M. *J. Fluid Mech.* (in the press).
12. Olson, P. & Christensen, U. *J. geophys. Res.* (submitted).

Metasomatic mineral titanate complexing in the upper mantle

Stephen E. Haggerty*, A. J. Erlank† & Ian E. Grey‡

* Department of Geology, University of Massachusetts, Amherst, Massachusetts 01003, USA
† Department of Geochemistry, University of Cape Town, Rondebosch 7700, South Africa
‡ CSIRO Division of Mineral Chemistry, PO Box 124, Port Melbourne, Victoria, Australia 3207

The extent and expression of metasomatism in the upper mantle are contentious issues[1,2], although the process has gained widespread acceptance to account for the subsequent enrichment of previously depleted lithosphere[3,4]. Uncertainties exist in the origin and precise compositions of the fluids involved, as well as in the total inventory of introduced metasomatic elements (particularly silicate-incompatible Ti, Zr, Nb, REE (rare-earth elements), Ba, Sr, Rb, K and Na). Metasomatism is readily identified by the presence of phlogopite, and in the most advanced stages by K-richterite[4]. In K-richterite-bearing harzburgites, these characteristic minerals are accompanied by rutile, armalcolite and lindsleyite–mathiasite (LIMA) solid solution members[5] of the crichtonite mineral series[6]. The LIMA series is one upper mantle repository for silicate-incompatible elements, but the series is also specifically enriched in chromium (12–18 wt% Cr_2O_3). While it has been assumed[5,7] that Cr is immobilized in the depleted lithosphere as a restite element, either in residual garnet, pyroxene, or in chromian spinel, there has been no direct evidence for the source of Cr in LIMA. We show here that LIMA solid-solution members are derived from Cr-spinel through interaction with metasomatic fluids by formation of a magnetoplumbite mineral with up to 14 wt % BaO, and which is inferred to contain Ce^{4+}. Fluid compositions are heterogeneous and an increase in the variety of repositories for silicate-incompatible trace elements is demonstrated in the subcontinental lithosphere at depths <100 km.

Lindsleyite (Ba-specific) and mathiasite (K-specific) are two new minerals[5] in the crichtonite mineral series, $AM_{21}O_{38}$ (where A = large cations Ba, K, Sr, Pb, Na, Ca, REE and M = small cations Ti, Cr, Nb, Fe, Mg, Al, Mn, Zn, Zr) that develop in upper-mantle depleted harzburgites of subcontinental lithospheric origin. In their description of the new minerals, S.E.H. *et al.*[5] illustrated (their Fig. 1*b*) an assemblage of chromian spinel cores rimmed by lindsleyite and this assemblage prompted a more detailed study of spinel-forming reactions during metasomatism. Samples examined were collected from the waste dumps (Bultfontein Floors) of country rock and boulder-sized upper mantle xenolith concentrates that have resulted from early diamond mining in the Kimberley district of South Africa. One sample (BD-3096) is a complexly veined harzburgite. The substrate is dominated by coarse (~5 mm) equant crystals of olivine and orthopyroxene, and subordinate 1-3-mm laths of phlogopite and anhedral K-richterite. The two largest veins (3-5-mm width) are composed of K-richterite, with lesser and corroded olivine, diopside, phlogopite and opaque mineral oxides. Euhedral to subhedral lindsleyite (Fig. 1*a*) and rounded grains of chromian spinel are present as rare inclusions in phlogopite and K-richterite, both in substrate and in veins. Interstitial to olivine and orthopyroxene, but always closely associated with phlogopite and K-richterite, are abundant, irregularly shaped assemblages of opaque mineral oxides that are commonly amoeboidal and 1-3 mm in the longest dimension.

Five distinct minerals are identified in the opaque oxide mineral assemblage using high-resolution oil-immersion objectives and reflected light microscopy. Approximately equal proportions of chromian spinel and an unidentified mineral (phase N), rimmed by lindsleyite, coexist in a blocky fabric or in an